Title

Cathodoluminescence characterization of dislocations in gallium nitride using a transmission electron microscope

Journal

Journal of Applied Physics, 94(7)

ISSN

0021-8979

Authors

Yamamoto, N
Itoh, H
Grillo, V
et al.

Publication Date

2003-10-01

Peer reviewed

Cathodoluminescence characterization of dislocations in gallium nitride using a transmission electron microscope

N. Yamamoto,[a] H. Itoh, and V. Grillo
Department of Physics, Tokyo Institute of Technology, Tokyo 152-8551, Japan

S. F. Chichibu
Institute of Applied Physics and Graduate School of Pure and Applied Sciences, University of Tsukuba, Tsukuba, Ibaraki 305-8573, Japan; NICP, ERATO, Japan Science and Technology Corporation (JST), Tokyo 102-0071, Japan

S. Keller, J. S. Speck, S. P. DenBaars, U. K. Mishra, and S. Nakamura
Departments of Materials Engineering and Electrical and Computer Engineering, University of California, Santa Barbara, California 93106; NICP, ERATO, Japan Science and Technology Corporation (JST), Tokyo 102-0071, Japan

G. Salviati
IMEM-CNR Institute, Parma, Italy

(Received 28 March 2003; accepted 12 June 2003)

Cathodoluminescence technique combined with transmission electron microscopy (TEM-CL) has been used to characterize optical properties of dislocations in GaN epilayers. The dislocations act as nonradiative centers with different recombination rates. TEM-CL observation showed that even for the same Burgers vector of ***a***, the dislocations show different electrical activity depending on the direction of dislocation line, i.e., the edge-type dislocation parallel to the *c* plane is very active, while the screw-type one is less active. The simulation of the CL images gives us the information of parameters such as carrier lifetime and diffusion length. © *2003 American Institute of Physics.* [DOI: 10.1063/1.1598632]

I. INTRODUCTION

Gallium nitride (GaN) based materials are key materials for the fabrication of blue and green light emitting diodes and laser diodes. These devices work in spite of high density of threading dislocations, though it has been pointed out that the threading dislocations affect the function, lifetime and efficiency of the devices. So far many authors have studied the electrical and optical properties of dislocations in GaN, using cathodoluminescence (CL) imaging technique combined with a scanning electron microscope,[1–4] and scanning tunneling microscope.[5] There are two distinct emissions appearing in the CL spectrum from GaN layers grown on sapphire substrates, i.e., band edge (BE) emission and yellow band (YB) emission. The CL images of the BE emission showed that the threading dislocations act as nonradiative recombination centers. The early CL observations also showed the correlation between distribution of dislocations and the YB emission, which suggested that the YB emission originates from threading dislocation itself or point defects decollating the dislocations.[1] However, Dassonneville *et al.*[6] said that the dislocations are not responsible for the YB emission.

The dislocations in the GaN hexagonal lattice have three different Burgers vectors, ***a***, ***c***, and ***a***+***c***. Then threading dislocations running parallel to the *c* axis are classified into edge, screw and mixed types, respectively. Hino *et al.*[7] showed by using etching technique and photoluminescence measurement that the threading dislocations of the three types affect the luminescence property in different ways. They suggested that the screw dislocations act as strong nonradiative centers, while the edge dislocations do not act as nonradiative centers. Arslan and Browning[8] analyzed electron energy loss spectra of intrinsic dislocations, and concluded that those dislocations do not have any local electric state in the band gap, and the electrical activity at dislocations could be attributed to the segregation of dopants, impurities and vacancies. However, very few efforts have been made for investigating the optical properties of individual dislocations of different types, so knowledge of the optical properties related to the type of the dislocation is still limited.

In the present study we observed the monochromatic CL images and transmission electron microscopy (TEM) images of dislocations in a GaN epilayer using a transmission electron microscope combined with a CL detection system (TEM-CL). The TEM-CL technique has an advantage in high spatial resolution and ability to characterize internal defect structures.[9] The dislocations of various types showed different contrasts in the CL images taken by the BE emission. The characters of those dislocations were determined from the contrast analysis of dark field TEM images. The optical properties of individual dislocations were derived from the comparison between the CL and TEM images.

[a]Author to whom correspondence should be addressed; electronic mail: nyamamot@surface.phys.titech.ac.jp

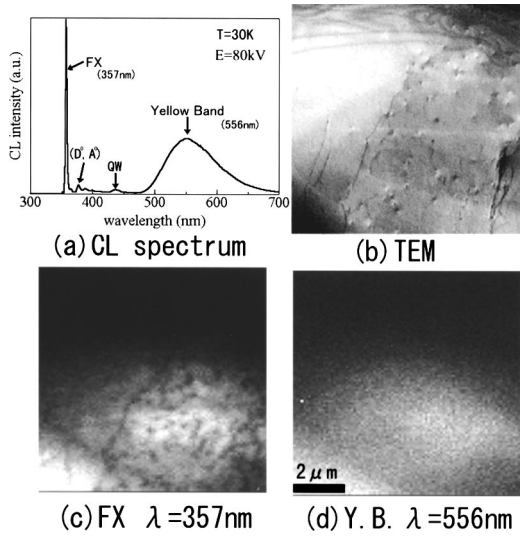

FIG. 1. (a) CL spectrum from a plan-view thin sample (T= 30 K, accelerating voltage= 80 kV), (b) TEM image, and monochromatic CL images of (c) FX and (d) YB luminescence.

II. EXPERIMENTS

We used a sample of an epitaxial lateral overgrowth (ELO) GaN layer with InGaN multiquantum wells (MQWs) grown on a sapphire substrate.[10] The width of a SiO_2 mask region deposited on the GaN buffer layer is 15 μm, and that of a window region is 5 μm. Density of the threading dislocations is nearly 10^{-10} cm^{-2} in the window region and 10^{-6} cm^{-2} in the wing region on the mask. The thickness of the undoped GaN ELO layer is 8 μm, and MQWs and a GaN cap layer a few nm thick are grown on the ELO layer. A plan-view TEM sample was made by Ar ion milling to remove the sapphire substrate and bottom part of the GaN epilayer.

III. RESULTS

Figure 1(a) shows a CL spectrum from a plan-view thin sample taken at 30 K with an accelerating voltage of 80 kV. A sharp peak at the wavelength of 357 nm is the BE emission associated with both free exciton (FX) and (D^0,X) bound exciton transitions,[11] and a broad peak at 556 nm is the yellow band (YB) emission. Other small peaks in between them are attributed to the donor to acceptor transition (D_0, A_0), and the emission from the InGaN MQWs (420 nm). Figure 1(b) shows a TEM image of a thin area, and Figs. 1(c) and 1(d) are monochromatic CL images of the same area taken at the peak wavelengths of BE and YB, respectively. Many threading dislocations are seen in the right region in Fig. 1(b) which corresponds to the window region of 5 μm in width. Several dislocations are seen running parallel to the surface at the boundary between the window and wing regions. Their line direction is nearly parallel to the $[01\bar{1}0]$ along the stripe of the SiO_2 mask. It is noticed that dark fine contrasts appear at some of the dislocations in the BE emission image of Fig. 1(c), which indicates that they act as nonradiative recombination centers. On the other hand, there is no fine contrast in the YB emission image of Fig. 1(d). The CL intensity distribution of the YB emission indicates thickness variation so that the thicker region gives a brighter contrast. The upper part of the image is dark because the specimen is thin in this area. It is noticed that the YB emission arises both in the window region and wing region around their boundary. This shows that the YB emission centers are not directly associated with the dislocations. The reason why no contrast arises at the dislocation in the CL image of YB can be attributed to the long lifetime of this radiative recombination process, which blurs the image contrast. This observation supports the idea that the YB emission originates from point defects such as a complex center associated with Ga vacancy and oxygen atoms.[12]

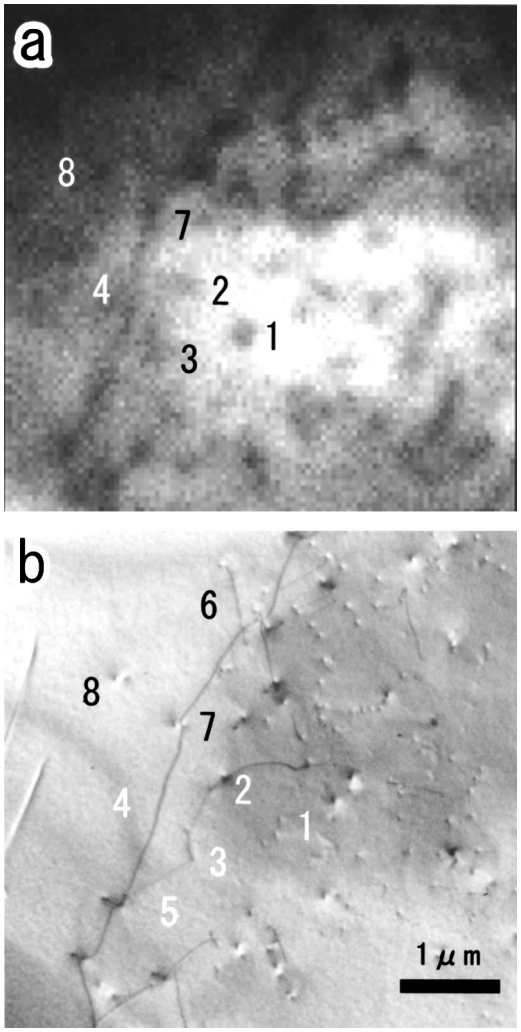

FIG. 2. (a) TEM image and (b) monochromatic CL image (FX) of a GaN thin film.

Figure 2(a) shows a magnified CL image (BE emission) of a 4.3×4.3 μm^2 area in Fig. 1(c) around the boundary between the window and wing regions. Figure 2(b) is a dark field TEM image of the same area taken under the excitation of the $(11\bar{2}0)$ reflection with the incidence direction nearly parallel to the *c* axis. The correspondence between the dark contrasts in the CL image of Fig. 2(a) and dislocations in Fig. 2(b) is apparent. However, some of the dark dot contrasts are due to several numbers of dislocations. To reveal the thread-

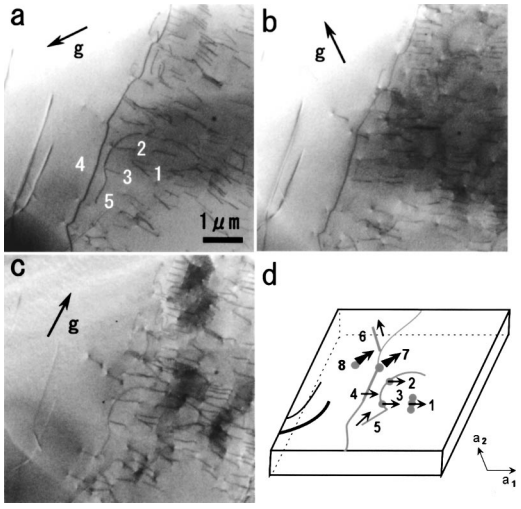

FIG. 3. Dark field TEM images of a GaN thin film taken by (a) $(\bar{1}01\bar{1})$, (b) $(\bar{1}10\bar{1})$ and (c) $(02\bar{2}0)$ reflections, respectively. (d) Schematic diagram of dislocation configuration. The Burgers vectors are indicated by arrows.

ing dislocations more clearly, a dark field TEM image of Fig. 3(a) was taken by the $(\bar{1}01\bar{1})$ reflection with tilting the sample by 31° from the incident beam direction. By measuring the length of the dislocation lines projected in the incident direction, the sample thickness can be derived to be 0.62 μm in this area. Typical dislocations concerned here are labeled 1–8. They are threading dislocations with dislocation lines parallel to the *c* axis except for No. 4 and No. 5 dislocations which run parallel to the surface or the *c* plane. Their Burgers vectors (***b***) were determined by the dark field technique using the simple invisibility rule ($\mathbf{g}\cdot\mathbf{b}=0$). Figures 3(b) and 3(c) are dark field TEM images taken by $(\bar{1}10\bar{1})$ and $(02\bar{2}0)$ reflections, respectively. No. 4 dislocation becomes invisible for the $(\bar{1}10\bar{1})$ reflection, and No. 5 dislocation becomes invisible for the $(02\bar{2}0)$ reflection. It is enough to observe dark field images for six different reflection vectors (***g***) in order to assign the Burgers vectors of all the dislocations, e.g., for the $\{20\bar{2}0\}$ and $\{10\bar{1}1\}$-type reflections. However, the invisibility rule is not always valid for the edge and mixed dislocations, because they involve $\mathbf{b}\times\mathbf{u}$ strain component, where $\mathbf{u}$ is an unit vector along the dislocation line. For the threading dislocation of edge typethe value of $\mathbf{g}\cdot\mathbf{b}\times\mathbf{u}$ is large, resulting in a visible contrast even for the reflections which satisfy the invisible rule. Nevertheless, it is practically possible to determine the Burgers vector by using this method. The Burgers vectors of the dislocations 1–8 are determined as listed in Table I, and schematically depicted in Fig. 3(d).

Most of the threading dislocations are edge-type dislocations with the Burgers vectors of $1/3\langle 11\bar{2}0\rangle(=\boldsymbol{a})$, as seen in Table 1 and Fig. 3(d). A few of the threading dislocations indicated Nos. 7 and 8 are mixed type with the Burgers vectors of $1/3\langle 11\bar{2}1\rangle(=\boldsymbol{a}+\boldsymbol{c})$, and no threading dislocation of screw type with the Burgers vector of $[0001](=\boldsymbol{c})$ was found in this area. A strong dark contrast labeled 1 in Fig. 2(a) comes from three threading dislocations of edge type, while separate single dislocations indicated Nos. 2 and 3

TABLE I. Properties of the dislocations. In the last column the CL contrast is indicated by symbols S (strong) and M (medium).

Disl. No.	Line	Burgers vector	Type	CL contrast
1	c	a_1	Edge	S
2, 3	c	a_1	Edge	M
4	[0110]	a_1	Edge	S
5	a_3	a_3	Screw	Invisible
6	a_2	a_2	Screw	Invisible
7, 8	c	a_3+c	Mixed	S

show a medium contrast. The threading dislocations of mixed type, Nos. 7 and 8, show the darker contrast compared to that of No. 2 dislocation. As for the dislocations running parallel to the surface, it is noticed that No. 4 dislocation, which is an edge type with the Burgers vector of $\boldsymbol{a}_1$, shows a strong contrast, while No. 5 and No. 6 dislocations, which are screw type with the Burgers vectors nearly parallel to the dislocation lines, show no contrast. This clearly reveals significant difference in electrical activity between the edge and screw dislocations with the same Burgers vector of ***a***.

CL intensity profiles across the dislocations, Nos. 1, 2, and 4 are shown in Fig. 4, in which they are smoothed digitally, and normalized by the intensity in the surrounding perfect region. The contrast given by the ratio between the intensities at the dislocation center and perfect region, $(I(P)-I(D)/I(P))$, is 0.39 for No. 1 dislocation (D1), 0.23 for No. 2 dislocation (D2) and 0.28 for No. 4 dislocation (D4), respectively. The full width at half maximum (FWHM) of each profile is 153 nm for D1, 147 nm for D2 and 188 nm for D4. These values were obtained from Gaussian fitting with the observed profiles.

IV. DISCUSSIONS

We studied the characteristic parameters of these dislocations by fitting the contrast with a trial and error method in

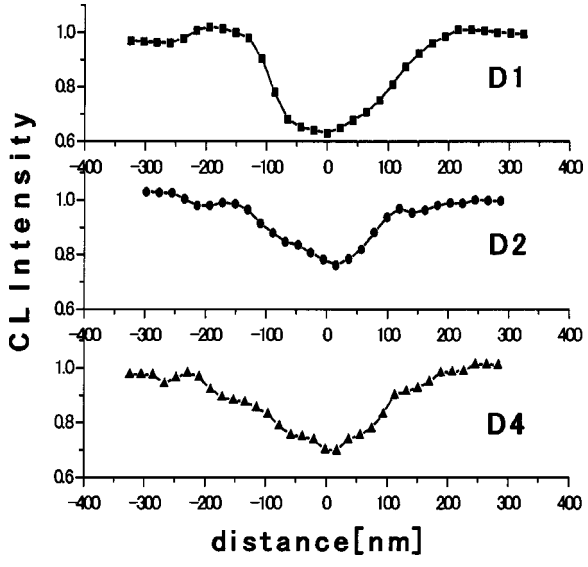

FIG. 4. CL intensity profiles along the dislocations; (a) the three TD dislocations (D1), (b) the single TD dislocation (D2), and (c) the edge dislocation (D4).

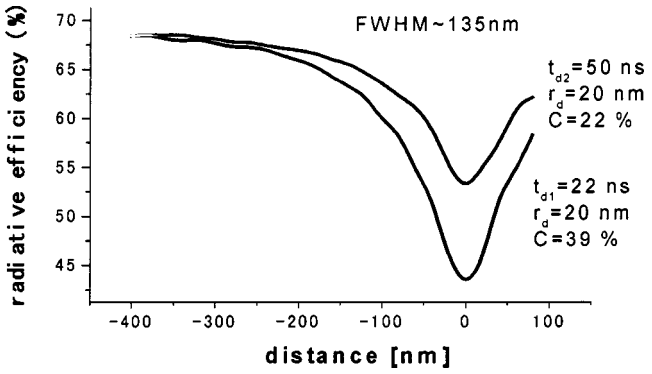

FIG. 5. Simulated CL intensity profiles along the dislocations of (a) D1 and (b) D2, using the parameters of diffusion length $L=158$ nm, and surface recombination rate $S=5\times10^4$ cm/s.

contrast simulations. These have been performed using a program recently developed by the co-authors based on the random walk method. For the simulation we assumed that the dislocation has a cylindrical shape with a radius of r_d, and a carrier lifetime is τ_d in it. We also took it into consideration that a surface recombination rate is set equal to $S=5\times10^4$ cm/s for both the upper and lower surfaces. According to the simulations the most important parameters determining contrast are diffusion length L and a parameter $\gamma=r_d^2/\tau_d$ related to the strength of the defect. Spurious dependence on each parameter of r_d and τ_d has been seen, but was neglected on first approximation. As already pointed out by other authors, dislocation contrast is nearly independent of diffusion length when it is large enough. On the contrary, this is particularly important in the case of GaN where this parameter is significantly small.

Figure 5 shows calculated profiles for dislocations penetrating a GaN thin plate with a thickness of 0.62 μm to fit with the profile of D1 and D2 in Fig. 4. As for the parameters, we fixed as $r_d=20$ nm and obtained the values of $\tau_{d1}=22$ ns and $\tau_{d2}=50$ ns for the dislocations D1 and D2. The width of the profile depends on the lifetime τ, thus on the diffusion length L ($L=\sqrt{D\tau}$), and the surface recombination rate S. In this simulation the diffusion length and surface recombination rate obtained from the fitting of the contrast and FWHM of the dislocations are $L=158$ nm and $S=5\times10^4$ cm/s. If taking a conventional lifetime of 1 ns, this implies that the diffusion constant D is equal to 0.25 cm^2/s. The diffusion length should be slightly shorter than this value, because we ignore the electron probe size of about 10 nm. By comparing between the τ_d values of D1 and D2, it is found that the change in τ_d is much smaller than a factor of 3, though the nonradiative recombination rate at the three threading dislocations of D1 is expected to be three times larger than that at the single one of D2. This suggests that the three dislocations of D1 do not effectively act as a sum of three nonradiative centers of the single dislocations.

The present value of diffusion length is smaller than the previously reported value of 250 nm by Rosner *et al.*,[2] who measured with Si-doped GaN at room temperature by SEM-CL. They used an exponentially decaying function to derive a diffusion length from the CL intensity profile. The present measurement was taken with an undoped GaN at 30 K, and thus the diffusion length is considered to be similar to their value. Sugawara *et al.*[3] obtained a small value of 50 nm from the SEM-CL observation in a similar way. But they used a thin film sample, and the surface recombination effect cannot be neglected. The FWHM of the dark spots in the CL image is comparable to those of the present one. Thus the value should be underestimated. From STL measurement Evoi *et al.*[5] also reported a small value of 30–55 nm. This could be reasonable from the fact that the sample is a highly doped one (2×10^{18} cm^{-2}), and the measurement was taken at low temperature. The diffusion length changes with doping concentration and temperature, and so we must be careful about comparison with those reported values.

We also calculated for a dislocation parallel to the surface located at various depth positions, and obtained a preliminary result that a dislocation contrast is a maximum at the central position and decreases as the dislocation position approaches the surfaces, though the change in contrast is little. The contrast of such a dislocation calculated with the same parameters used for the D2 dislocation in Fig. 5 is definitely smaller than that of the threading one in Fig. 5. This is reasonable because the defect region ($r_d=20$ nm) crossing the carrier generation region is smaller in this case than that of the threading dislocation elongating along the thickness direction by 0.62 μm. Therefore the strong contrast of the edge dislocation, D4, clearly indicates that the D4 dislocation is electrically more active than the threading edge dislocation, D2. It is also evident that the difference in contrast between the edge and screw dislocations in Fig. 2 cannot be due to the difference in depth position, but should be attributed to the intrinsic properties of them.

The difference in contrast is considered to originate from the dislocation core structures, even when the dislocations have the same Burgers vector of $\boldsymbol{a}$. The threading dislocation of edge type has dangling bonds at the core, which exist on the Ga and N atoms along the dislocation line parallel to the c direction. Jones[13] predicted that the threading dislocation of the edge type generates a shallow level state in the energy gap, and is electrically inactive. However, the edge dislocation with a line parallel to the $[01\bar{1}0]$ direction has dangling bonds only at the Ga atoms or the N atoms at the core, similar to the case of the 60° dislocation (the α and β types) in zinc blend structure. Therefore it could be possible that the edge dislocation of this type has a deep level state in the energy gap, and becomes electrically more active. As for the screw dislocation, the theoretical calculations suggested that the threading dislocation with the Burgers vector of $\boldsymbol{c}$ causes large strain field to provide a deep level state in the band gap, and becomes electrically active. However, the screw dislocation parallel to the c plane with the Burgers vector of $\boldsymbol{a}$ has relatively small strain field and no dangling bonds, and then could be electrically less active. Unfortunately, the theoretical calculation of electric states for the dislocations running parallel to the c plane has not been made yet. As another possibility we should consider the effect of impurities, because they combine with Ga or N vacancy at the dislocation

core to form complex centers, and affect electrical activity.[14] This will be examined in a future study using fresh dislocations.

V. SUMMARY

Cathodoluminescence technique combined with transmission electron microscopy (TEM-CL) has been applied to characterize optical properties of dislocations in GaN epilayers. Here we observed CL images of an edge-type threading dislocation, and edge and screw dislocations running parallel to the (0001) surface, which have the same Burgers vector of ***a***. Those dislocations act as nonradiative centers with different recombination rates, showing different contrasts. We found that the edge-type dislocation parallel to the *c* plane is more active than the edge-type threading dislocation, while the screw-type one is inactive. This indicates different electrical activities of those dislocations depending on the direction of dislocation line. The simulation of the CL images gives us the information on parameters such as carrier lifetime and diffusion length. The diffusion length of undoped GaN is estimated to be 158 nm at 30 K.

ACKNOWLEDGMENTS

This work was supported in part by the 21st Century COE Program ''Promotion of Creative Interdisciplinary Materials Science for Novel Functions'' under the Ministry of Education, Culture, Sports, Science and Technology of Japan and AOARD/AFOSR.

[1] F. A. Ponce, D. P. Bour, and W. Gotz, Appl. Phys. Lett. **68**, 57 (1996).
[2] S. J. Rosner, E. C. Carr, M. J. Ludowise, G. Girolami, and H. I. Erikson, Appl. Phys. Lett. **70**, 420 (1997).
[3] T. Sugawara, H. Sato, M. Hao, Y. Naoi, S. Kurai, S. Tottori, K. Yamashita, K. Nishino, L. Romano, and S. Sakai, Jpn. J. Appl. Phys., Part 2 **37**, L398 (1998).
[4] M. Hao, S. Mahanty, T. Sugawara, Y. Morishita, H. Takenaka, J. Wang, S. Tottori, K. Nishino, Y. Naoi, and S. Sakai, J. Appl. Phys. **85**, 6497 (1999).
[5] S. Evoi, C. K. Harnett, H. G. Craighead, T. J. Eustis, W. A. Davis, M. J. Murphy, W. J. Schaff, and L. F. Eastman, J. Vac. Sci. Technol. B **16**, 1943 (1998).
[6] S. Dassonneville, A. Amokrane, B. Sieber, J.-L. Farvacque, B. Beaumont, and P. Gibart, J. Appl. Phys. **89**, 3736 (2001).
[7] T. Hino, S. Tomiya, T. Miyajima, K. Yanashima, S. Hashimoto, and M. Ikeda, Appl. Phys. Lett. **76**, 3421 (2000).
[8] I. Arslan and N. D. Browning, Phys. Rev. B **65**, 075310 (2002).
[9] T. Mitsui, N. Yamamoto, T. Tadokoro, and S. Ohta, J. Appl. Phys. **80**, 6972 (1996).
[10] S. Chichibu, H. Marchand, M. S. Minsky, S. Keller, P. T. Fini, J. P. Ibbetson, S. B. Fleischer, J. S. Speck, J. E. Bowers, E. Hsu, U. K. Mishra, S. P. Denbaars, T. Deguchi, T. Sota, and S. Nakamura, Appl. Phys. Lett. **74**, 1460 (1999).
[11] S. Chichibu, H. Okumura, S. Nakamura, G. Feuillet, T. Azuhata, T. Sota, and S. Yoshida, Jpn. J. Appl. Phys., Part 1 **36**, 1976 (1997).
[12] G. Salviati, M. Albrecht, C. Zanotti-Fregonara, N. Armani, M. Mayer, Y. Shreter, M. Guzzi, Y. V. Melnik, K. Vassilevski, V. A. Dmitriev, and H. P. Strunk, Phys. Status Solidi A **171**, 325 (1999).
[13] R. Jones, Mater. Sci. Eng., B **71**, 24 (2001).
[14] J. Elsner, R. Jones, M. I. Heggie, S. Oberg, and P. R. Briddon, Phys. Rev. B **58**, 12571 (1998).